

Chemical Science

Accepted Manuscript

This article can be cited before page numbers have been issued, to do this please use: Q. Li, T. Jiang, S. Yang, J. Chai, H. Yu and M. Zhu, *Chem. Sci.*, 2025, DOI: 10.1039/D5SC06282A.



This is an Accepted Manuscript, which has been through the Royal Society of Chemistry peer review process and has been accepted for publication.

Accepted Manuscripts are published online shortly after acceptance, before technical editing, formatting and proof reading. Using this free service, authors can make their results available to the community, in citable form, before we publish the edited article. We will replace this Accepted Manuscript with the edited and formatted Advance Article as soon as it is available.

You can find more information about Accepted Manuscripts in the [Information for Authors](#).

Please note that technical editing may introduce minor changes to the text and/or graphics, which may alter content. The journal's standard [Terms & Conditions](#) and the [Ethical guidelines](#) still apply. In no event shall the Royal Society of Chemistry be held responsible for any errors or omissions in this Accepted Manuscript or any consequences arising from the use of any information it contains.

ARTICLE

Construction of a homologous series of metal nanoclusters and its implications for structure-activity correlations

Qinzen Li,^{†a,b} Tingting Jiang,^{†b} Sha Yang,^b Jinsong Chai,^{*a,b} Haizhu Yu^{*b} and Manzhou Zhu^{*b}Received 00th January 20xx,
Accepted 00th January 20xx

DOI: 10.1039/x0xx00000x

The precise structures of metal nanoclusters (NCs) can serve as accurate model for the establishment of structure-activity correlation, thereby attracting attention as a new type of heterogeneous catalyst. However, it remains challenging to definitively establish the relationship between the structure of local sites on NCs and catalytic activity. Herein, a homologous series of metal NCs were constructed for the structure-activity correlation. Four NCs including Au₂₄(SAdm)₁₄(OPDP)₁ (**Au₂₄**), Au₂₃Cd₁(SR)₁₄(OPDP)₁Cl (**Au₂₃Cd₁**), Au₂₂Cd₂(SAdm)₁₄(OPDP)₁Cl₂ (**Au₂₂Cd₂**) and Au₂₁Cd₃(SAdm)₁₃(OPDP)₁Cl₂ (**Au₂₁Cd₃**) (HSAdm = 1-adamantanethiol; OPDP = (oxydi-2,1-phenylene)bis(diphenylphosphine)) were synthesized. These four NCs exhibit the same common Au₂₁M₁(SR)₁₀(OPDP)₁ (M = Au/Cd) structural skeleton but two different surface motifs. These two motifs in the four NCs exhibit regular evolution mode, that is, 2[Au₁(SR)₂] for **Au₂₄**, [Au₁(SR)₂] + [Cd₁(SR)₃Cl] for **Au₂₃Cd₁**, 2[Cd₁(SR)₃Cl] for **Au₂₂Cd₂**, and [Cd₁(SR)₃Cl] + [CdCl] for **Au₂₁Cd₃**. Electrocatalytic oxygen reduction reaction (ORR) is performed with these four NCs as catalyst, revealing a catalytic activity sequence of **Au₂₁Cd₃** > **Au₂₂Cd₂** > **Au₂₃Cd₁** > **Au₂₄**. Based on their differences in surface motifs, the structure-activity relationship can be rigorously correlated to the certain motif types, showing an activity sequence of [CdCl] > [Cd₁(SR)₃Cl] > [Au₁(SR)₂]. Moreover, compared with the other three NCs, **Au₂₁Cd₃** showed a higher electron transfer number and a smaller Tafel slope in catalyzing ORR, indicating a different kinetic reaction process and higher reactivity of [CdCl] than [Cd₁(SR)₃Cl] and [Au₁(SR)₂], which revealed a configuration effect in determining catalytic activity of NCs.

Introduction

As an important catalytically active materials in the field of nanocatalysis, metal nanoparticle catalysts have received extensive attention because it presents the advantages of high turnover in homogeneous catalysis and recyclability in heterogeneous catalysis.^{1–3} Understanding the catalytic mechanism and revealing the structure-activity relationship are of great significance for their performance improvement, upgrading and iteration.^{4–6} Relevant mechanism studies have shown that specific local structural sites of metal nanoparticles, such as crystal facets and defects,^{7,8} play a decisive role in determining the catalytic activity, but due to the difficulties in the precise structural characterization of the active site, more detailed mechanism discovery and the establishment of accurate structure-activity relationships are still challenging.

Nanoclusters (NCs), have shown their unique advantages in correlating structure-activity because the precise structures of them can serve as an accurate research model for the mechanism study and avoid the error caused by the structure simulation.^{9–15} Nevertheless, the structural diversity among NCs (including differences in metal cores, surface motifs, and ligand types)^{16–19} greatly reduces their structural comparability, making it difficult to accurately correlate their structure-activity relationships. In this regard, NCs that bearing single structural variable were singled out to construct comparable systems and simplify the research models for structure-activity correlation. For the part of metal core, size-dependent activity was revealed by comparing the catalytic effect between Au NCs with different size (Scheme 1a).^{20–24} Moreover, with the construction of alloyed counterparts from the same parent NC, the doping effect on catalytic activity can be well elucidated,^{25,26} which can even reach the level of single atom (Scheme 1b).^{27–31} On the other hand, ligand effect on the catalytic activity has also been investigated by changing the ligand type on the surface of the certain NCs (Scheme 1c).^{32–36} However, surface motifs (or local sites) of NCs, as an important origin of their catalytic activity,^{37–39} their configuration effect on catalytic activity have not been systematically studied due to the difficulty of constructing NC series bearing only difference in the configuration of local sites. Heterometal doping is a widely used implementation strategy to regulate the molecular compositions of the parent NCs.^{40–45} Among the common heterometal types for doping parent Au NCs, Cd has shown its great potential in regulating the local

^aSchool of Materials Science and Engineering, Anhui University, Hefei, Anhui 230601, China.

^bDepartment of Chemistry and Centre for Atomic Engineering of Advanced Materials, Key Laboratory of Structure and Functional Regulation of Hybrid Materials of Ministry of Education, Institutes of Physical Science and Information Technology and Anhui Province Key Laboratory of Chemistry for Inorganic/Organic Hybrid Functionalized Materials, Anhui University, Hefei, Anhui 230601, China.

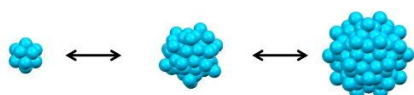
*E-mail: chajis@ahu.edu.cn (J.C.); yuhaizhu@ahu.edu.cn (H.Y.); zzmz@ahu.edu.cn (M.Z.)

[†]Electronic Supplementary Information (ESI) available: Supporting figures, and tables. Crystallographic information for Au₂₄, Au₂₂Cd₂ and Au₂₁Cd₃ (CIF). CCDC 2374164, 2128986, and 2341165. See DOI: 10.1039/x0xx00000x

‡ These authors contributed equally to this work.



a) Size effect



b) Doping effect

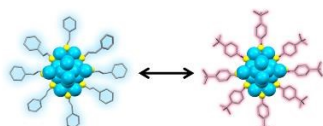
Doping type



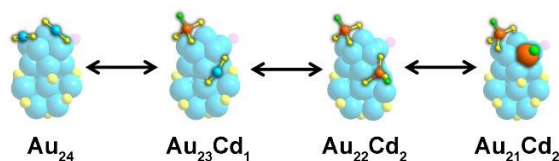
Doping degree



c) Ligand effect



d) This work: Structure effect from local sites



Scheme 1. Schematic representation of NC series for investigating structure-activity relationship: (a) NCs with different size; (b) NCs doped with different types (or numbers) of heterometal atoms; (c) NCs protected by different types of ligands; (d) NCs with same skeleton but different local motifs.

structure of NCs due to the diversity of its doping modes in Au NCs. Cd can be doped into the different parts of the NCs, including surface motif, core surface and core center,⁴⁶ which allows it to construct specific Cd-doping sites in NCs with distinct structural configurations. More importantly, the introduction of Cd atoms can achieve local structural regulation while maintaining the basic skeleton of the parent Au NCs.⁴⁷⁻⁴⁹ In addition to this, the as-introduced Cd atoms in Au NCs can serve as active sites for further catalytic reactions,^{47,50,51} which will be beneficial to the study of its structure-activity relationship. Inspired by this, we expect to obtain a series of structural analogues by controlling the doping process of Cd atoms in Au NCs, so as to establish an accurate structure-activity relationship by correlating their structural and performance differences.

Herein, taking a newly synthesized $\text{Au}_{24}(\text{SAdm})_{14}(\text{OPDP})_1$ (**Au₂₄**, HSAdm = 1-adamantanethiol; OPDP = (oxydi-2,1-phenylene)bis(diphenylphosphine)) as parent NCs, three Au-Cd alloying NCs were constructed via a controlled stepwise Cd-doping process, formulated as $\text{Au}_{23}\text{Cd}_1(\text{SAdm})_{14}(\text{OPDP})_1\text{Cl}$ (**Au₂₃Cd₁**), $\text{Au}_{22}\text{Cd}_2(\text{SAdm})_{14}(\text{OPDP})_1\text{Cl}_2$ (**Au₂₂Cd₂**), and $\text{Au}_{21}\text{Cd}_3(\text{SAdm})_{13}(\text{OPDP})_1\text{Cl}_2$ (**Au₂₁Cd₃**), respectively. Single crystal X-ray diffraction (SC-XRD) reveals that these three Au-Cd

NCs exhibit a high degree of structural homology with **Au₂₄** and show significant structural continuity (Scheme 1d). That is, all the four NCs exhibit the same $\text{Au}_{21}\text{M}_1(\text{SR})_{10}(\text{OPDP})_1$ ($\text{M} = \text{Au}/\text{Cd}$) structural skeleton, which is composed of a Au_{15}M_1 kernel, two $\text{Au}_1(\text{SR})_2$, one bridged SR, one $\text{Au}_4(\text{SR})_5$, and one OPDP ligand. Anchored on this common skeleton, the remaining two surface motifs in these four NCs show regular evolution, that is, two $\text{Au}_1(\text{SR})_2$ for **Au₂₄**, one $\text{Au}_1(\text{SR})_2$ and one $\text{Cd}_1(\text{SR})_3\text{Cl}$ for **Au₂₃Cd₁**, two $\text{Cd}_1(\text{SR})_3\text{Cl}$ for **Au₂₂Cd₂**, one $\text{Cd}_1(\text{SR})_3\text{Cl}$ and one CdCl for **Au₂₁Cd₃**. Taking these four nanocluster homologues as research platform, the relationship between oxygen reduction reaction (ORR) electrocatalytic activity and precise structure was established unambiguously, which demonstrated a configuration effect of the local sites on catalytic activity. That is, a catalytic activity sequence of $[\text{CdCl}] > [\text{Cd}_1(\text{SR})_3\text{Cl}] > [\text{Au}_1(\text{SR})_2]$.

Results and discussion

As the parent Au NCs for constructing structural homologues, **Au₂₄** was synthesized via a two-phase ligand exchange method.⁵² Pure **Au₂₄** can be obtained by separating the raw product with a thin-layer chromatography plate. UV-vis spectroscopy showed a series of characteristic peaks located at 343, 364, 391, 452, 494, 582, 678, and 750 nm, respectively (Fig. 1a). Electrospray mass spectrometry (ESI-MS) in positive mode showed an intense signal at 3803.3 Da (Fig. 1b), which can be assigned into the formula $\text{Au}_{24}(\text{SAdm})_{14}(\text{OPDP})_1$ that bearing +2 charge (calculated position: 3803.3 Da). The well-matched isotopic pattern between experimental and calculated data further supports this molecular composition. The atomically precise structure is the key information necessary to study the structural evolution of NCs. So, X-ray single crystal diffraction was employed to figure out its molecular structure. **Au₂₄** crystallizes in the monoclinic $\text{P}2_1/\text{c}$ group with four NCs in one unit cell (Fig. 1a, inset; Table S1). **Au₂₄** was revealed to exhibit a Au_{16} kernel, which can be regarded as the combination of one icosahedral Au_{13} and one tetrahedral Au_4 by sharing a vertex atom. As shown in Fig. 1c, the icosahedron and tetrahedron unit in the kernel was connected by one bridging thiolate and two $\text{Au}_1(\text{SR})_2$ motifs and one $\text{Au}_4(\text{SR})_5$ was found to bind on the bottom of icosahedral Au_{13} unit and surround the Au_4 unit. Further, two more $\text{Au}_1(\text{SR})_2$ and one diphosphine ligand was anchored on the top side of the Au_{16} kernel, forming the complete **Au₂₄** NCs.

CdCl_2 was first reacted with **Au₂₄** to proceed the Cd-doping process. However, no any new species generated in this reaction, instead, **Au₂₄** was decomposed in 6 h (Fig. S1). Further attempt via reacting **Au₂₄** with both CdCl_2 and HSAdm successfully triggered the doping process, and a **Au₂₃Cd₁** NC can be isolated. Its crystal structure (reported in our previous work)⁴⁶ is similar to the parent **Au₂₄** NCs, that they bear the same structural skeleton. Besides, they show differences in their motifs located on the top of the Au_{16} kernel, at which the two $\text{Au}_1(\text{SR})_2$ in **Au₂₄** were reconstructed as one $\text{Cd}_1(\text{SR})_3\text{Cl}$ and one new $\text{Au}_1(\text{SR})_2$ in **Au₂₃Cd₁** (Fig. S2). The structural transformation from **Au₂₄** to **Au₂₃Cd₁** was investigated using time-dependent UV-vis spectroscopy and ESI-MS (Fig. 2, I). Time-dependent UV-vis spectroscopy revealed a gradual



ARTICLE

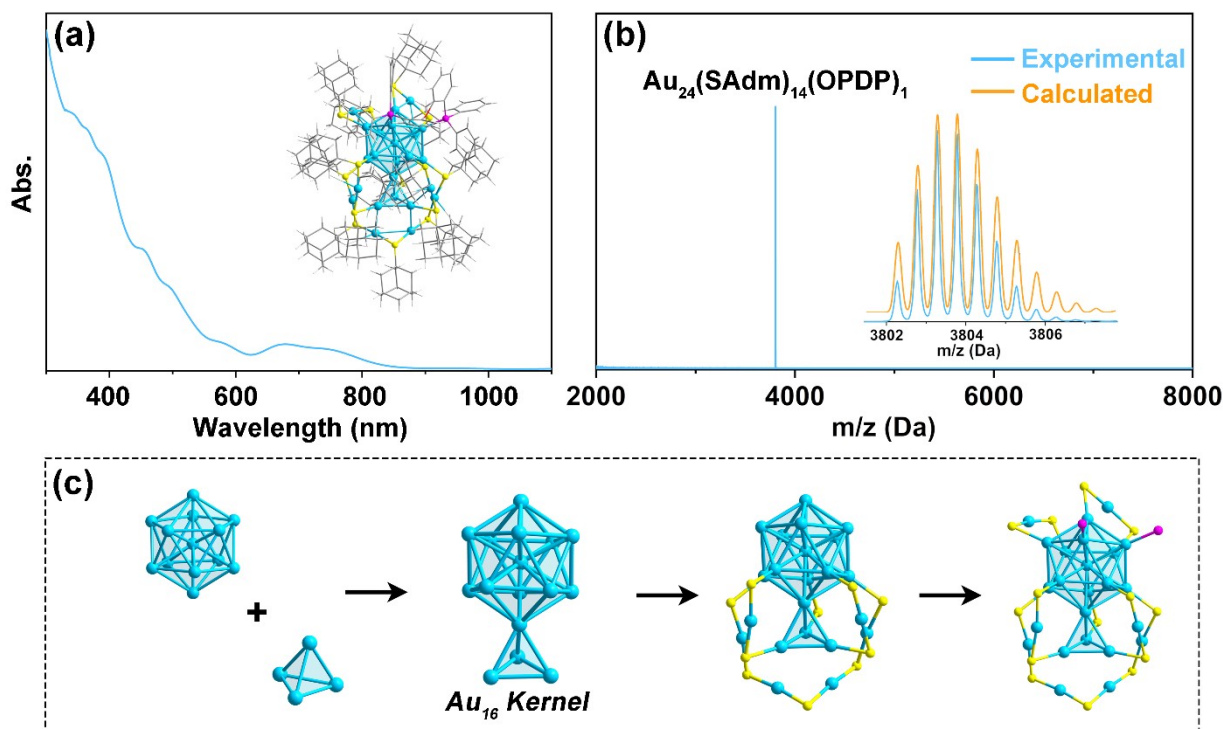


Fig. 1 (a) UV-vis spectrum of the Au_{24} . Inset: total structure of Au_{24} . (b) ESI-MS of Au_{24} . Inset: experimental and calculated isotopic patterns of the MS signal. (c) Structural analysis of the skeleton in Au_{24} . (Label: light blue = Au; yellow = S; magenta = P; gray = C; red = O; white = H)

attenuation of the characteristic peak belonging to Au_{24} and a set of new peaks located at 520, 600, 650, and ~ 770 nm emerged. At the same time, changes in the reaction components were also monitored by ESI-MS. The results showed that, along with the weakening of the Au_{24} signal, the a peak located at 7522.5 Da belonging to $[\text{Au}_{23}\text{Cd}_1(\text{SAdm})_{14}(\text{OPDP})_1]^+$ gradually increased. These observations demonstrated that the Au_{24} can convert into $\text{Au}_{23}\text{Cd}_1$ by introducing Cd species. After 6 h, the signal of Au_{24} became invisible, indicating that Au_{24} has been completely converted.

Interestingly, after all Au_{24} were converted to $\text{Au}_{23}\text{Cd}_1$, it was found that further extension of the reaction time would result in the formation of another new species, showing a signal located at 7473.5 Da in ESI-MS (Fig. S3). Considering that the addition of CdCl_2 (20 equivalent of Au_{24}) in the reaction is excessive, this phenomenon may suggest that $\text{Au}_{23}\text{Cd}_1$ is not the final state of the reaction, and it can continue to undergo structural transformation. Based on this conjecture, $\text{Au}_{23}\text{Cd}_1$ was isolated and purified as the reactant to mix with CdCl_2 and HSA dm. As a result, time-dependent UV-vis spectroscopy

revealed a transformation in absorption peaks from that of $\text{Au}_{23}\text{Cd}_1$ to three new peaks located at 560, 660 and 760 nm. Further ESI-MS analysis revealed a newly emerged signal at 7473.5 Da and the reaction ended after about 36 h. This signal peak matched well with the formula $[\text{Au}_{22}\text{Cd}_2(\text{SAdm})_{14}(\text{OPDP})_1\text{Cl}]^+$, indicating the additional doping of another Cd atom in the $\text{Au}_{23}\text{Cd}_1$ NCs (Fig. 2, II).

The acquisition of $\text{Au}_{22}\text{Cd}_2$ motivated us to investigate whether it could further undergo a structural transformation process. Therefore, $\text{Au}_{22}\text{Cd}_2$ was treated with the same reaction condition as that for Au_{24} and $\text{Au}_{23}\text{Cd}_1$, however, $\text{Au}_{22}\text{Cd}_2$ keep unchanged under this condition. It was noted that the reaction rate from $\text{Au}_{23}\text{Cd}_1$ to $\text{Au}_{22}\text{Cd}_2$ slowed down significantly compared with the reaction from Au_{24} to $\text{Au}_{23}\text{Cd}_1$ (36 h vs. 6 h), implying that the reaction between the $\text{Au}_{22}\text{Cd}_2$ and Cd might be more difficult. So, the reaction temperature was elevated to promote any possible transformation process. At a reaction temperature of 55 $^\circ\text{C}$, it was found that $\text{Au}_{22}\text{Cd}_2$ can slowly transform into another species. Time-dependent UV-vis spectroscopy showed a blue shift in the absorption peaks and ESI-MS revealed that the newly formed NCs exhibited a signal



ARTICLE

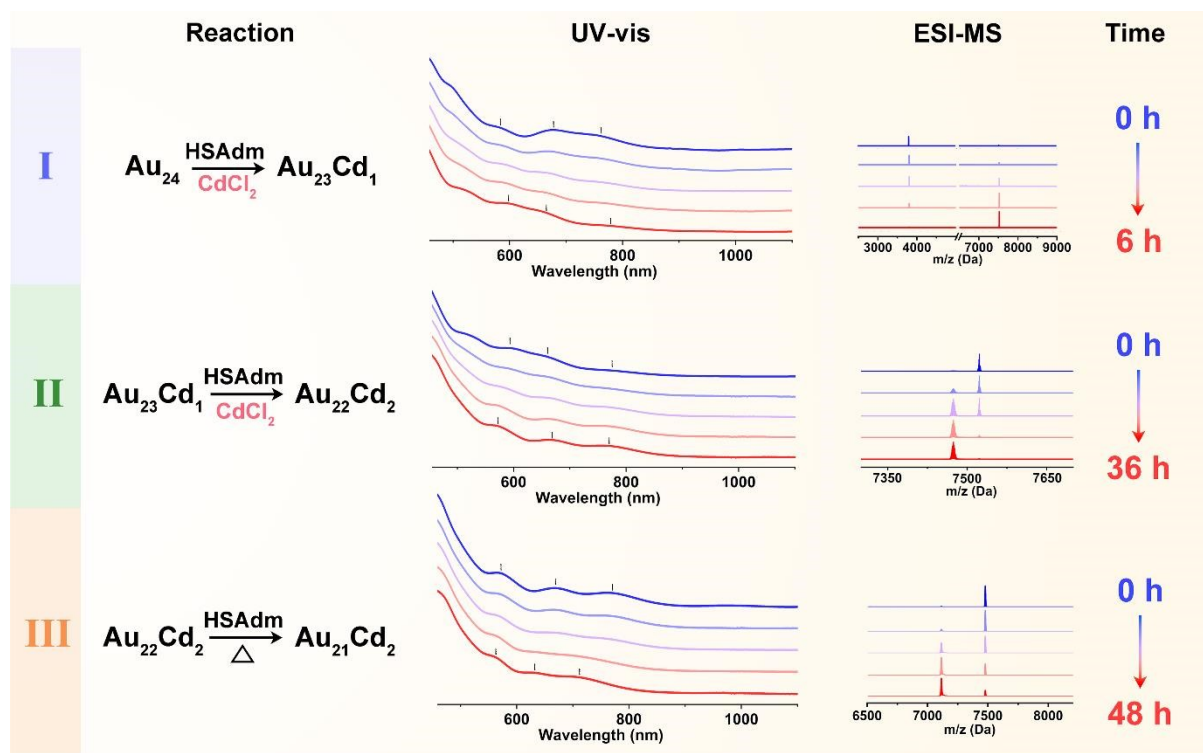


Fig. 2 Reaction system composition and the time-dependent UV-vis spectra and ESI-MS of the three transformation stages, including **Au₂₄** to **Au₂₃Cd₁** (stage I), **Au₂₃Cd₁** to **Au₂₂Cd₂** (stage II), **Au₂₂Cd₂** to **Au₂₁Cd₂** (stage III).

peak located at 7109.5 Da (Fig. 2, III). This peak position corresponds to the molecular formula of $[\text{Au}_{21}\text{Cd}_2(\text{SAdm})_{13}(\text{OPDP})_1\text{Cl}]^+$. In this case, the doping number of Cd atoms did not change from **Au₂₂Cd₂** to **Au₂₁Cd₂**, indicating that it is not a doping process. Thus, we removed the CdCl_2 from the reaction and found that the transformation can still happen. The transformation from **Au₂₂Cd₂** to **Au₂₁Cd₂** showed a quite low reaction rate and there will be some untransformed **Au₂₂Cd₂** in the final system. Further attempt to trigger the structural transformation of **Au₂₁Cd₂** with Cd-doping or heat treatment did not yield any new species (Fig. S4), demonstrating that the **Au₂₁Cd₂** was a stable product that can be regarded as the final state of this entire transformation pathway (**Au₂₄** \rightarrow **Au₂₃Cd₁** \rightarrow **Au₂₂Cd₂** \rightarrow **Au₂₁Cd₂**). This process can be also observed intuitively by the thin-layer chromatography separation (Fig. S5).

To unravel the structural relationship between these NCs, the atomically precise structures of the other two NCs, **Au₂₂Cd₂** and **Au₂₁Cd₂**, were solved with SC-XRD (Tables S2-3). Interestingly, all the four NCs including **Au₂₄**, **Au₂₃Cd₁**, **Au₂₂Cd₂** and **Au₂₁Cd₂** were revealed to exhibit a high degree of structural homology. As shown in Fig. 3, all the four NCs exhibit an Au_{15}M_1 ($\text{M} = \text{Au}/\text{Cd}$)

kernel that protected by one $\text{Au}_4(\text{SR})_5$, one bridging thiolate, one diphosphine and two $\text{Au}_1(\text{SR})_2$ with the same binding site. Apart from this shared structure unit, there are four binding sites left on the surface of the Au_{15}M_1 kernel, structural differences of these four NCs were found to exist in these positions. For **Au₂₄**, two adjacent $\text{Au}_1(\text{SR})_2$ motifs was found to bind on these four remaining coordination sites. After the doping of one Cd atom in the **Au₂₄**, **Au₂₃Cd₁** was formed and the motifs at this site change into a $\text{Cd}_1(\text{SR})_3\text{Cl}$ unit and a new $\text{Au}_1(\text{SR})_2$. Further doping of Cd resulted in the formation of two $\text{Cd}_1(\text{SR})_3\text{Cl}$ motifs in the **Au₂₂Cd₂**. Finally, in **Au₂₁Cd₂**, one of the Cd atoms collapses into the core surface, forming a $\text{Au}_{15}\text{Cd}_1$ kernel with configuration maintained, and one $\text{Cd}_1(\text{SR})_3\text{Cl}$ and one Cl were anchored on that four binding sites. UV-vis spectra and ESI-MS of **Au₂₃Cd₁**, **Au₂₂Cd₂**, and **Au₂₁Cd₂** solution obtained by dissolving their crystal samples were subsequently recorded, which revealed the consistent absorption peaks and formula (Fig. S6) with the previous results (Fig. 2) and crystal structures. To understand the role of Cd in constructing structure homologue, the reaction system (containing **Au₂₄**, CdCl_2 and HSA dm initially) were traced by mass spectrometry to clarify the



ARTICLE

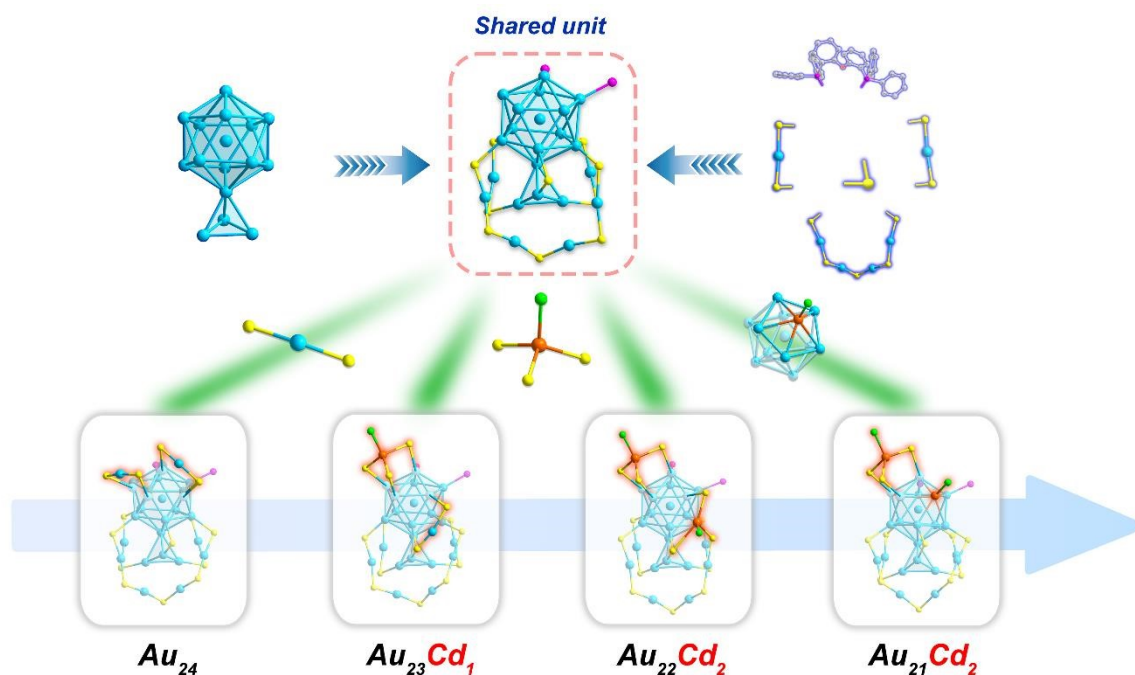


Fig. 3 Illustration of the shared structural unit in Au_{24} , $\text{Au}_{23}\text{Cd}_1$, $\text{Au}_{22}\text{Cd}_2$ and $\text{Au}_{21}\text{Cd}_2$, and the movement trajectory of Cd atoms in NCs as the doping process progresses. (Label: light blue = Au; orange = Cd; bright green = Cl; yellow = S; magenta = P; gray = C; red = O)

existence form of the introduced Cd element and the removed gold atom. For the initial state, a significant signal peak belonging to the $[\text{CdCl}]^+$ species was detected in the reaction system. After the transformation from Au_{24} to $\text{Au}_{23}\text{Cd}_1$, $\text{Au}_1(\text{SR})_2^-$ can be probed in the reaction solution (Fig. S7). This result indicated that $[\text{CdCl}]^+$ was the important species to trigger the doping process, while the substituted gold atom generated as the form of $\text{Au}_1(\text{SR})_2^-$. The capture of $\text{Au}_1(\text{SR})_2^-$ species explains why the thiolate ligand is necessary for triggering the structural conversion, that is, thiolate ligands act as stabilizer for the substituted gold atoms, thus facilitating the reaction.

DFT calculations were then employed to reveal the pathway throughout the entire structural transformation process with a ligand-simplified model (Fig. S8).⁵³ Given that the $\text{Au}_1(\text{SR})_2$ motif in Au_{24} will convert into a $\text{Cd}_1(\text{SR})_3\text{Cl}$ motif in $\text{Au}_{23}\text{Cd}_1$, two possible pathways that can achieve this motif transition, that is, a $\text{Au}_1(\text{SR})_2$ motif infusion process and a $[\text{CdCl}]$ substitution process were considered. As shown in Fig. S9, the energy barrier of these two processes were calculated, respectively. The result showed that the $[\text{CdCl}]$ substitution process was a more energetically favorable process, demonstrating that the replacement of Au atom by $[\text{CdCl}]$ unit is the triggering step of the transformation from Au_{24} to $\text{Au}_{23}\text{Cd}_1$. The calculated

pathway indicated a $[\text{CdCl}]$ insertion and $\text{Au}_1(\text{SR})_2$ rearrangement processes (Fig. S10a, Fig. S11). For the second stage, from $\text{Au}_{23}\text{Cd}_1$ to $\text{Au}_{22}\text{Cd}_2$, it can be achieved in one step by the substitution of Au atom with a $[\text{CdCl}]$ unit (Fig. S10b). As showed in Fig. S12, the spatial position of two SR from the $\text{Au}_1(\text{SR})_2$ and one SR from the $\text{Au}_4(\text{SR})_5$ together form a suitable doping site for the construction of a $\text{Cd}_1(\text{SR})_3\text{Cl}$ motif in tetrahedral geometry. The existence of this special site may be the key to facilitate the Cd-doping reaction. In the third stage, the $\text{Au}_{22}\text{Cd}_2$ was found to transform into the final product $\text{Au}_{21}\text{Cd}_2$ via undergoing two intermediate states (Fig. S10c). In the first step, the $[\text{CdCl}]$ unit of $\text{Cd}_1(\text{SR})_3\text{Cl}$ motif in $\text{Au}_{22}\text{Cd}_2$ collapses downward into the surface of the Au_{13} icosahedron unit in kernel, forming the $\text{Au}_{13}\text{Cd}_1$ core unit. This $\text{Au}_{13}\text{Cd}_1$ intermediate state then reverts to the $\text{Au}_{12}\text{Cd}_1$ icosahedron with the extrusion of one Au atom, forming the final $\text{Au}_{21}\text{Cd}_2$ NCs. This calculated result is consistent with the fact that $\text{Au}_{22}\text{Cd}_2$ can convert into $\text{Au}_{21}\text{Cd}_2$ without the addition of extra Cd source. That is, with the combination of the atomically precise structures and calculated transformation pathway, the evolutionary rule for this homologous series of NCs can be summarized as two continuous processes: the gradual increase of Cd doping number and the outward to inward transfer of Cd

ARTICLE

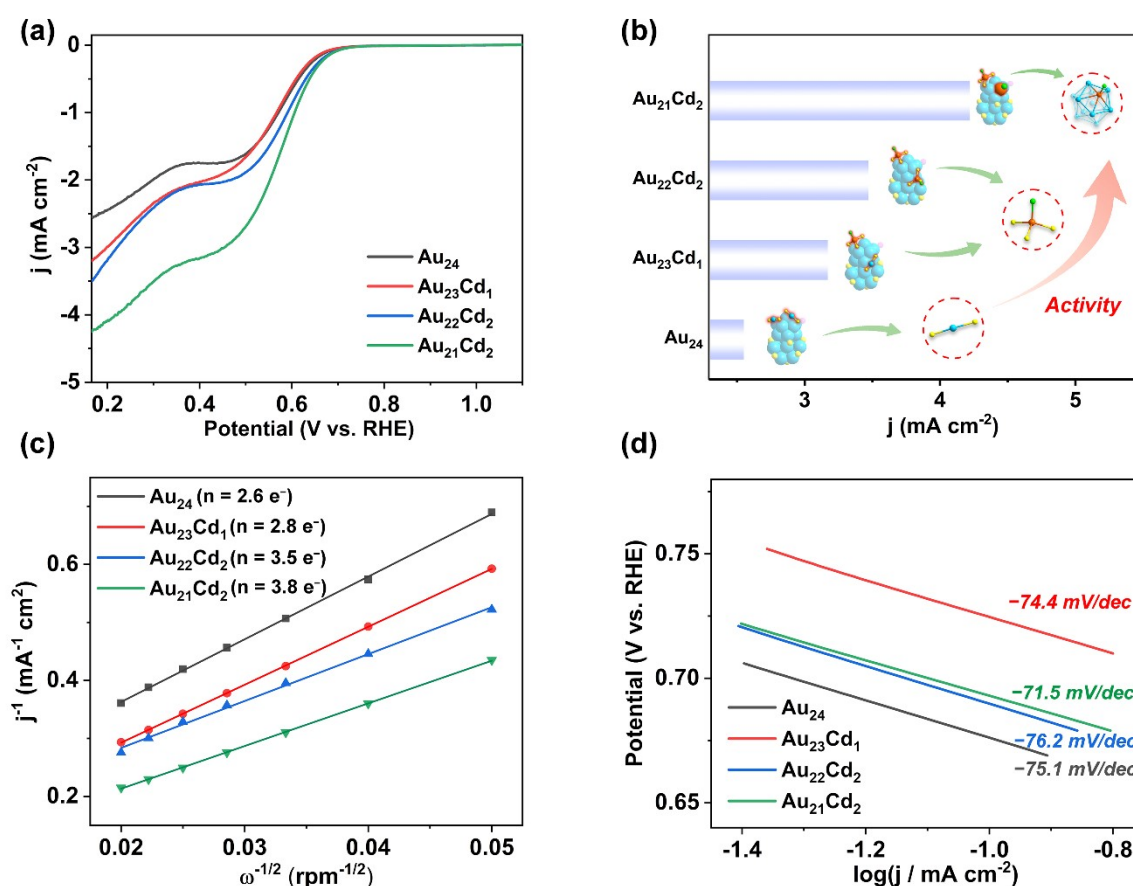


Fig. 4 (a) ORR polarization curves for different NCs as catalysts obtained in O_2 -saturated 0.1 mol/L KOH solutions at 1600 rpm. (b) The current density values for different NCs as catalysts (0.17 V, 1600 rpm) and the corresponding different local structures of these NCs. (c) Koutecky–Levich plots (j^{-1} vs. $\omega^{-1/2}$) of different NCs. (d) Corresponding Tafel plots of the NCs.

substitution site, which is manifested as the gradual replacement of $\text{Au}_1(\text{SR})_2$ by $\text{Cd}_1(\text{SR})_3\text{Cl}$ motifs, and the subsequent collapse of $\text{Cd}_1(\text{SR})_3\text{Cl}$ into the core-anchored CdCl unit.

The structural similarity endows these nanocluster homologues to serve as a unique research platform for studying and establishing their structure-activity correlation while excluding the influence of size and ligand effects. As shown in Fig. S13, all the four NCs display similar absorption characteristics within the short-wavelength region (<450 nm), which is attributed to their similar kernel structures, and the differences in their motifs primarily affect the positions of absorption peaks at long wavelengths. Then, their photoluminescence properties were also evaluated. As shown in Fig. S14, only Au_{24} exhibits weak near-infrared photoluminescence at ~ 1000 nm while the other three NCs do not have photoluminescence performance.

Furthermore, electrocatalytic ORR activity were evaluated using the four NCs as catalysts (Fig. 4a, Fig. S15). All the four NCs were loaded on the activated carbon as the electrocatalysts (Fig. S16) and the ORR tests were performed with these four electrocatalysts under the same condition. As shown in Fig. 4a, the current density displayed a gradual increasing trend with a sequence as $\text{Au}_{24} < \text{Au}_{23}\text{Cd}_1 < \text{Au}_{22}\text{Cd}_2 < \text{Au}_{21}\text{Cd}_2$.

The acquisition of the precise structures of these four nanocluster homologues allow us to accurately correlate their structure-activity relationships based on their local structural differences. The ORR current density for Au_{24} and $\text{Au}_{23}\text{Cd}_1$ was revealed as 2.55 and 3.17 mA cm^{-2} (0.17 V, 1600 rpm), respectively. Given that their only structural difference lies in two surface motifs, that is, Au_{24} has two $\text{Au}_1(\text{SR})_2$ while $\text{Au}_{23}\text{Cd}_1$ exhibits one $\text{Cd}_1(\text{SR})_3\text{Cl}$ and one $\text{Au}_1(\text{SR})_2$, one can easily draw the conclusion that the newly form $\text{Cd}_1(\text{SR})_3\text{Cl}$ motif in $\text{Au}_{23}\text{Cd}_1$ can serve as a more active catalytic sites in ORR than $\text{Au}_1(\text{SR})_2$.

motif. In addition, **Au₂₂Cd₂** (with two Cd₁(SR)₃Cl motifs on the surface) display a current density of 3.47 mA·cm⁻² under the same condition, showing a slight enhancement in the catalytic activity when compared with that of **Au₂₃Cd₁** (bearing one Cd₁(SR)₃Cl), indicating that the as-formed second Cd₁(SR)₃Cl unit in **Au₂₂Cd₂** can improve the catalytic performance to some extent by increasing the active site. Furthermore, a more significant change in current density can be observed for **Au₂₁Cd₂** (4.22 mA·cm⁻²). Since that there is only one structural difference between **Au₂₂Cd₂** and **Au₂₁Cd₂**, that is, a Cd₁(SR)₃Cl motif of **Au₂₂Cd₂** changes into a CdCl unit that collapsed in the kernel in **Au₂₁Cd₂**, this result demonstrated that the enhanced catalytic activity for **Au₂₁Cd₂** can be attributed to this change in the doping position and configuration of the Cd atom. That is, the catalytic activity sequence was clearly revealed as [CdCl]>[Cd₁(SR)₃Cl]>[Au₁(SR)₂] (Fig. 4b). It shows that the Cd-containing structural sites are more active than the Au-containing unit, which was probably caused by breaking of the Cd-Cl bond than can expose the coordination site for the combination between Cd atom and substrate molecule. As evidence, the dissociation of Cl atoms can be observed in all the ESI-MS results of the three Au-Cd NCs (**Au₂₃Cd₁**, **Au₂₂Cd₂** and **Au₂₁Cd₂**) in this work (Fig. S6). After the removal of Cl atom from CdCl and Cd₁(SR)₃Cl, the active sites for these two cases are the icosahedral Au₁₂Cd₁ and the Cd₁(SR)₃ unit, respectively. Considering the higher stability of the icosahedral structure, it will be more conducive to the dissociation of Cl atom and the removal of product molecule from the active sites during catalysis, thus explaining the higher catalytic activity of CdCl than Cd₁(SR)₃Cl.

More importantly, the transformation of local configurations of active sites from Cd₁(SR)₃Cl to CdCl shows a significant effect on catalytic activity. The overall transferred electrons were calculated according to the Koutecky–Levich plots (Fig. 4c), demonstrating equivalent ORR electron transfer numbers of *n* = 2.6, 2.8, and 3.5 for **Au₂₄**, **Au₂₃Cd₁**, and **Au₂₂Cd₂**, respectively. This indicates **Au₂₄**, **Au₂₃Cd₁**, and **Au₂₂Cd₂** reduced O₂ through a combination of 2 e⁻ and 4 e⁻ processes. An electron transfer number of *n* = 3.8 e⁻ was revealed for **Au₂₁Cd₂**, indicating a dominant four-electron reduction process for it. It indicated that the incorporation of Cd in **Au₂₄** can change the reaction mechanism from 2 e⁻ to 4 e⁻ process and the core-doping type of Cd in **Au₂₁Cd₂** show the most remarkable effect. Besides, Tafel plots revealed similar slope values for **Au₂₄**, **Au₂₃Cd₁**, and **Au₂₂Cd₂** at ~75 mV/dec, while a smaller slope value (71.5 mV/dec) for **Au₂₁Cd₂** is observed (Fig. 4d), demonstrating a higher kinetic reaction rate for the CdCl unit in it. The above results unambiguously demonstrated that changing the configuration of the active site in the NCs is a powerful means to enhance the catalytic activity by changing the kinetics and reaction mechanism of the catalytic reaction.

Conclusions

In this study, a homologous series of metal NCs including **Au₂₄**, **Au₂₃Cd₁**, **Au₂₂Cd₂** and **Au₂₁Cd₂**, was constructed via a controlled stepwise Cd-doping process. These four NCs differ from each

other in structure by only two surface motifs. Structural analysis revealed that a regular structural evolution pattern in these NCs, which showed as the gradual conversion from Au₁(SR)₂ to Cd₁(SR)₃Cl motifs, and finally the CdCl unit inserting in icosahedral kernel. The structure continuity of this set of nanocluster structure homologous was further used to study the relationship between its local sites and the catalytic performance. A ORR catalytic activity sequence of **Au₂₄**<**Au₂₃Cd₁**<**Au₂₂Cd₂**<**Au₂₁Cd₂** was revealed. By combining the catalytic results and the precise structures of NCs, the structure-activity relationship was unambiguously revealed, showing an activity sequence of [CdCl]>[Cd₁(SR)₃Cl]>[Au₁(SR)₂] in local structural sites. In addition, Koutecky–Levich and Tafel plots demonstrated that the as-formed [CdCl] unit in **Au₂₁Cd₂** can lead to a dominant four-electron reduction pathway and smaller Tafel slope when compared with other three NCs, showing the important role of structural configuration in local sites on determining the reaction mechanism and kinetics for nanocluster catalysts. This work has systematically studied the relationship between surface configuration of local sites and catalytic activity through the construction of nanocluster structure homologues, which offers a new perspective for the study of structure-activity relationship in NCs.

Author Contributions

All authors have given approval to the final version of the manuscript. Q. L. executed the experimental synthesis, characterization, and data analysis. T. J. and H. Y. carried out the theoretical calculations. Q. L. carried out single-crystal X-ray diffraction data collection, structure refinement; Q. L., T. J. and S. Y. prepared the first draft of the manuscript and all authors contributed to the preparation of the manuscript. J. C., H. Y., and M. Z. supervised the project.

Data availability

The data supporting this article have been included as part of the ESI. Crystallographic data for **Au₂₄**, **Au₂₂Cd₂** and **Au₂₁Cd₂** have been deposited at the CCDC under 2374164, 2128986 and 2341165, respectively.

Conflicts of interest

There are no conflicts to declare.

Acknowledgements

We acknowledge financial support of the National Natural Science Foundation of China (22371003, 22301001, U24A20480, U23A2090), the Ministry of Education, and the Anhui Provincial Natural Science Foundation (2308085QB40). The numerical calculations in this paper have been done on Hefei advanced computing center.



References

- C. Gao, F. Lyu and Y. Yin, *Chem. Rev.*, 2021, **121**, 834–881.
- C. Xie, Z. Niu, D. Kim, M. Li and P. Yang, *Chem. Rev.*, 2020, **120**, 1184–1249.
- Z. Li, S. Ji, Y. Liu, X. Cao, S. Tian, Y. Chen, Z. Niu and Y. Li, *Chem. Rev.*, 2020, **120**, 623–682.
- D. Leybo, U. J. Etim, M. Monai, S. R. Bare, Z. Zhong and C. Vogt, *Chem. Soc. Rev.*, 2024, **53**, 10450–10490.
- L. Liu and A. Corma, *Chem. Rev.*, 2023, **123**, 4855–4933.
- J. D. Lee, Miller, J. B., A. V. Shneidman, L. Sun, J. F. Weaver, J. Aizenberg, J. Biener, J. A. Boscoboinck, A. C. Foucher, A. I. Frenkel, J. E. S. van der Hoeven, B. Kozinsky, N. Marcella, M. M. Montemore, H. T. Ngan, C. R. O'Connor, C. J. Owen, D. J. Stacchiola, E. A. Stach, R. J. Madix, P. Sautet and C. M. Friend, *Chem. Rev.*, 2022, **122**, 8758–8808.
- Y. Kang, S. M. João, R. Lin, K. Liu, L. Zhu, J. Fu, W.-C. Cheong, S. Lee, K. Frank and B. Nickel, *Nat. Commun.*, 2024, **15**, 3923.
- C. Xie, D. Yan, H. Li, S. Du, W. Chen, Y. Wang, Y. Zou, R. Chen and S. Wang, *ACS Catal.*, 2020, **10**, 11082–11098.
- Y. Du, H. Sheng, D. Astruc and M. Zhu, *Chem. Rev.*, 2020, **120**, 526–622.
- R. Jin, G. Li, S. Sharma, Y. Li and X. Du, *Chem. Rev.*, 2021, **121**, 567–648.
- Z.-J. Guan, J.-J. Li, F. Hu and Q.-M. Wang, *Angew. Chem., Int. Ed.*, 2022, **61**, e202209725.
- K. Xiao, Y. Xue, B. Yang and L. Zhao, *CCS Chem.*, 2021, **3**, 555–565.
- W.-D. Tian, W.-D. Si, S. Havenridge, C. Zhang, Z. Wang, C. M. Aikens, C.-H. Tung and D. Sun, *Sci. Bull.*, 2024, **69**, 40–48.
- W.-D. Si, C. Zhang, M. Zhou, W.-D. Tian, Z. Wang, Q. Hu, K.-P. Song, L. Feng, X.-Q. Huang, Z.-Y. Gao, C.-H. Tung and D. Sun, *Sci. Adv.*, 2023, **9**, eadg3587.
- W.-D. Si, C. Zhang, M. Zhou, Z. Wang, L. Feng, C.-H. Tung and D. Sun, *Sci. Adv.*, 2024, **10**, eadm6928.
- S.-S. Zhang, L. Feng, R. D. Senanayake, C. M. Aikens, X.-P. Wang, Q.-Q. Zhao, C.-H. Tung and D. Sun, *Chem. Sci.*, 2018, **9**, 1251–1258.
- Y. Li, T. Higaki, X. Du and R. Jin, *Adv. Mater.*, 2020, **32**, 1905488.
- Y. Li, M. Zhou and R. Jin, *Adv. Mater.*, 2021, **33**, 2006591.
- B. Zhang, J. Chen, Y. Cao, O. J. H. Chai and J. Xie, *Small*, 2021, **17**, 2004381.
- S. Li, X. Du, Z. Liu, Y. Li, Y. Shao and R. Jin, *Precis. Chem.*, 2023, **1**, 14–28.
- Y. Liu, H. Tsunoyama, T. Akita, S. Xie and T. Tsukuda, *ACS Catal.*, 2011, **1**, 2–6.
- G. Li, D.-e. Jiang, S. Kumar, Y. Chen and R. Jin, *ACS Catal.*, 2014, **4**, 2463–2469.
- Y. Sun, E. Wang, Y. Ren, K. Xiao, X. Liu, D. Yang, Y. Gao, W. Ding and Y. Zhu, *Adv. Funct. Mater.*, 2019, **29**, 1904242.
- Y. Zhang, P. Song, T. Chen, X. Liu, T. Chen, Z. Wu, Y. Wang, J. Xie and W. Xu, *Proc. Natl. Acad. Sci. U. S. A.*, 2018, **115**, 10588.
- G. Li, X. Sui, X. Cai, W. Hu, X. Liu, M. Chen, Y. Zhu, *Angew. Chem., Int. Ed.*, 2021, **60**, 10573–10576.
- X. Liu, E. Wang, M. Zhou, Y. Wan, Y. Zhang, H. Liu, Y. Zhao, J. Li, Y. Gao and Y. Zhu, *Angew. Chem., Int. Ed.*, 2022, **61**, e202207685.
- K. Kwak, W. Choi, Q. Tang, M. Kim, Y. Lee, D.-e. Jiang and D. Lee, *Nat. Commun.*, 2017, **8**, 14723.
- Y. Liu, X. Chai, X. Cai, M. Chen, R. Jin, W. Ding and Y. Zhu, *Angew. Chem., Int. Ed.*, 2018, **57**, 9775–9779.
- Y. Li, H. K. Kim, R. D. McGillicuddy, S.-L. Zheng, K. J. Anderton, G. J. Stec, J. Lee, D. Cui and J. A. Mason, *J. Am. Chem. Soc.*, 2023, **145**, 9304–9312.
- S. Su, Y. Zhou, L. Xiong, S. Jin, Y. Du and M. Zhu, *Angew. Chem. Int. Ed.*, 2024, **57**, e202404629.
- S. Masuda, H. Hirai, P. Zhao, S. Takano, M. Ehara and T. Tsukuda, *ACS Catal.*, 2024, **14**, 17123–17131.
- X.-K. Wan, J.-Q. Jia, Z.-A. Nan and Q.-M. Wang, *Sci. Adv.*, 2017, **3**, e1701823. DOI: 10.1039/D5SC06282A
- Z. Liu, H. Tan, B. Li, Z. Hu, D.-e. Jiang, Q. Yao, L. Wang and J. Xie, *Nat. Commun.*, 2023, **14**, 3374.
- M. Bodiuzzaman, K. Murugesan, P. Yuan, B. Maity, A. Sagadevan, N. Malenahalli H, S. Wang, P. Maity, M. F. Alotaibi, D.-e. Jiang, M. Abulikemu, O. F. Mohammed, L. Cavallo, M. Rueping and O. M. Bakr, *J. Am. Chem. Soc.*, 2024, **146**, 26994–11781.
- Z. Liu, J. Chen, B. Li, D.-e. Jiang, L. Wang, Q. Yao and J. Xie, *J. Am. Chem. Soc.*, 2024, **146**, 11773–27005.
- S. M. Han, M. Park, J. Kim and D. Lee, *Angew. Chem. Int. Ed.*, 2024, **63**, e202404387.
- J. Chai, S. Yang, Y. Lv, H. Chong, H. Yu and M. Zhu, *Angew. Chem. Int. Ed.*, 2019, **58**, 15671–15674.
- Y. Tan, G. Sun, T. Jiang, D. Liu, Q. Li, S. Yang, J. Chai, S. Gao, H. Yu and M. Zhu, *Angew. Chem., Int. Ed.*, 2024, **63**, e202317471.
- J.-Q. Fan, Y. Li, W. W. Xu and M.-B. Li, *Angew. Chem., Int. Ed.*, 2025, **64**, e202413861.
- X. Kang, Y. Li, M. Zhu and R. Jin, *Chem. Soc. Rev.*, 2020, **49**, 6443–6514.
- H. Hirai, S. Takano, T. Nakashima, T. Iwasa, T. Taketsugu and T. Tsukuda, *Angew. Chem., Int. Ed.*, 2022, **134**, e202207290.
- Z. Liu, M. Zhou, L. Luo, Y. Wang, E. Kahng and R. Jin, *J. Am. Chem. Soc.*, 2023, **145**, 19969–19981.
- W.-Q. Shi, L. Zeng, R.-L. He, X.-S. Han, Z.-J. Guan, M. Zhou and Q.-M. Wang, *Science*, 2024, **383**, 326–330.
- A. Pniakowska, K. K. Ramankutty, P. Obstarczyk, M. P. Bakulić, Ž. S. Maršić, V. Bonačić-Koutecký, T. Bürgi and J. Olesiak-Bańska, *Angew. Chem., Int. Ed.*, 2022, **61**, e202209645.
- S. Zhuang, D. Chen, L. Liao, Y. Zhao, N. Xia, W. Zhang, C. Wang, J. Yang and Z. Wu, *Angew. Chem., Int. Ed.*, 2020, **59**, 3073–3077.
- Y. Tan, Y. Lv, L. Xu, Q. Li, J. Chai, S. Yang, H. Yu and M. Zhu, *J. Am. Chem. Soc.*, 2023, **145**, 4238–4245.
- Q. Li, K. J. Lambright, M. G. Taylor, K. Kirschbaum, T.-Y. Luo, J. Zhao, G. Mpourmpakis, S. Mokashi-Punekar, N. L. Rosi and R. Jin, *J. Am. Chem. Soc.*, 2017, **139**, 17779–17782.
- W. Zhang, S. Zhuang, L. Liao, H. Dong, N. Xia, J. Li, H. Deng and Z. Wu, *Inorg. Chem.*, 2019, **58**, 5388–5392.
- X. Liu, G. Yao, X. Cheng, J. Xu, X. Cai, W. Hu, W. W. Xu, C. Zhang and Y. Zhu, *Chem. Sci.*, 2021, **12**, 3290–3294.
- L. Xu, Q. Li, T. Li, J. Chai, S. Yang and M. Zhu, *Inorg. Chem. Front.*, 2021, **8**, 4820–4827.
- J.-Q. Fan, Y. Yang, C.-B. Tao and M.-B. Li, *Angew. Chem., Int. Ed.*, 2023, **62**, e202215741.
- Q. Li, S. Yang, T. Chen, S. Jin, J. Chai, H. Zhang and M. Zhu, *Nanoscale*, 2020, **12**, 23694–23699.
- S. Yang, S. Chen, L. Xiong, C. Liu, H. Yu, S. Wang, N. L. Rosi, Y. Pei and M. Zhu, *J. Am. Chem. Soc.*, 2018, **140**, 10988–10994.



The data supporting this article have been included as part of the ESI. Crystallographic data for Au₂₄, Au₂₂Cd₂ and Au₂₁Cd₂ have been deposited at the CCDC under 2374164, 2128986 and 2341165, respectively.

[View Article Online](#)

DOI: 10.1039/D5SC06282A

